Subgrid-scale modelling in relaminarizing flows

IOP PUBLISHING FLUID *DYNAMICS* RESEARCH

Fluid Dyn. Res. **42** (2010) 045510 (14pp) doi:10.1088/0169-5983/42/4/045510

Subgrid-scale modelling in relaminarizing flows

Ugo Piomelli[1] **and Carlo Scalo**

Department of Mechanical and Materials Engineering, Queen's University, Kingston, ON, Canada

E-mail: ugo@me.queensu.ca

Received 6 October 2009, in final form 26 March 2010
Published 7 May 2010
Online at stacks.iop.org/FDR/42/045510

Communicated by M Maxey

Abstract

The reversion of a turbulent flow to a laminar or quasi-laminar state may take very different paths, depending on the cause of the relaminarization; modelling these flows is quite difficult. Large-eddy simulations (LES) may be quite effective as the large, momentum-carrying eddies are accurately resolved; the unresolved, subgrid-scale (SGS) stresses, however, may still play an important role. We report here the results of an *a priori* analysis of the behaviour of the SGS stresses in two relaminarizing flows: a plane channel subjected to spanwise rotation, and a boundary layer subjected to a strong favourable pressure gradient resulting in freestream acceleration. The *a priori* test results are accompanied by actual LES, which highlight the effect of grid resolution and modelling errors on the dynamics of the relaminarization. Dynamic SGS models predict the overall features of the relaminarization correctly, although some of the details are not captured. At the levels of grid refinement used, however, the SGS contribution to momentum transport is very small, and little difference is observed between the results obtained with the various models.

1. Introduction

The transition to turbulence of a laminar flow has received, historically, a great deal of attention; the case of a turbulent flow that reverts to a laminar state has been less frequently studied. This problem, however, is quite important in applications, since relaminarization can be observed, for instance, in stratified, rotating or accelerating boundary layers. An important feature of relaminarizing flows is the fact that in most cases turbulent fluctuations do not vanish completely, although they may be significantly reduced. It is often the correlation between streamwise and wall-normal fluctuations that decreases, reducing

[1] Author to whom any correspondence should be addressed.

0169-5983/10/045510+14$30.00

turbulent momentum transport and production of turbulent kinetic energy, rather than the turbulent energy itself: turbulent motions persist, but become inactive. Understanding the state of the relaminarized flow in these cases is very important: once the cause of the relaminarization is removed, the flow re-transitions to turbulence through a process that may depend critically on the residual turbulence levels during relaminarization.

Both transitioning and relaminarizing flows pose significant modelling challenges: turbulence models for the Reynolds-averaged Navier–Stokes (RANS) equations are usually based on high-Reynolds-number turbulence physics, and are often unable to predict the non-equilibrium state that characterizes these flows without ad hoc adjustments. Subgrid-scale (SGS) models for large-eddy simulations (LES) are also based on high-Reynolds-number physics, and do not include transitional effects; some models, however, have the property of giving vanishing eddy-viscosity when the flow is laminar. Several types of SGS models have this property, and can be expected to be applicable to simulations of this type. Among them are models based on dynamic modelling ideas (Germano *et al* 1991), the spectral-dynamic model (Lamballais *et al* 1998) and models based on approximate deconvolution (Domaradzki and Adams 2002).

In LES, however, grid resolution becomes an issue, especially in laminar-to-turbulent transition: the instability mechanisms must be resolved by the mesh itself, which may require very significant computational resources. The simulation must, in such cases, approach the resolution of a direct numerical simulations (DNS), since coarse meshes tend to promote early transition. Voke and Yang (1995), for instance, performed LES of bypass transition over a flat plate using a modification of the Smagorinsky–Lilly model (Smagorinsky 1963, Lilly 1967) that allowed the viscosity to vanish in low-Reynolds-number regions of the flow, and obtained good agreement with experimental data. Ovchinnikov *et al* (2004), however, observed that when the mesh is refined, the transition point moves downstream of the experimental location; a very careful specification of the freestream turbulence and a finer grid than that used by Voke and Yang (1995) are required to match the experimental data in grid-converged calculations.

In relaminarizing flows, the grid requirements are less stringent than in transitional cases, since the turbulent eddies tend to become more elongated, and the smallest eddies are dissipated first. The SGS model, however, must still be able to account for the factors causing relaminarization properly; very dissipative models, for instance, are expected to result in excessively rapid relaminarization.

In this work, we will consider LES of relaminarizing flows, with the goal of studying the behaviour of the eddy viscosity and the grid requirements necessary to achieve accurate results. In their review article, Narasimha and Sreenivasan (1979) consider various mechanisms for reversion to a laminar state, and distinguish cases in which the turbulent kinetic energy (TKE) decays during the relaminarization process from those in which it remains 'frozen', while the wall-normal and horizontal velocity components become decorrelated. This results in decreased Reynolds stresses and, consequently, decreased production of turbulent kinetic energy. Here, we will examine one problem from each of these two classes: the reversion to laminar flow due to rotation, and the relaminarization in a turbulent boundary layer subjected to strong acceleration. By performing well-resolved DNS we will be able to verify the accuracy of the LES, and also to understand the physics of the energy transfer from large to small scales, and the requirements that SGS models must satisfy to give accurate results in these cases. This goal shall be achieved by performing *a priori* tests, in which the DNS data are filtered and the 'exact' SGS stresses, forces and dissipation are computed, and by *a posteriori* comparison of the DNS data with the actual LES results.

2. Problem formulation

The governing equations solved in this problem are either the incompressible flow equations of conservation of mass and momentum, or their filtered counterpart:

$$\frac{\partial \overline{u}_j}{\partial x_j} = 0, \tag{1}$$

$$\frac{\partial \overline{u}_i}{\partial t} + \frac{\partial \overline{u}_j \overline{u}_i}{\partial x_j} = \nu \frac{\partial^2 \overline{u}_i}{\partial x_j \partial x_j} - \frac{1}{\rho}\frac{\partial \overline{p}}{\partial x_i} - \frac{\partial \tau_{ij}}{\partial x_j} + \delta_{i1} f - 2\epsilon_{i3k}\Omega_3 \overline{u}_k. \tag{2}$$

In the channel, Ω_3 is the rotation about the spanwise (x_3 or z) axis and f a forcing term that is applied to maintain a constant flow rate in the channel (neither of these terms is used in the boundary-layer simulations). The SGS stresses, $\tau_{ij} = \overline{u_i u_j} - \overline{u}_i \overline{u}_j$, are modelled using either the plane-averaged (DEV) (Germano *et al* 1991, Lilly 1992) or the Lagrangian-averaged dynamic eddy-viscosity model (LDEV) (Meneveau *et al* 1996).

For the channel, boundary conditions are periodic in the streamwise (x_1 or x) and spanwise directions (x_3 or z). No-slip conditions are used at the walls. In the accelerating boundary layer, periodic boundary conditions are used only in the spanwise direction. At the inflow, the recycling/rescaling method by Lund *et al* (1998) is used, while at the outflow a convective condition is applied (Orlanski 1976). At the freestream, a profile of the streamwise time-averaged velocity $U_\infty(x)$ is assigned; the mean freestream wall-normal velocity component, $V_\infty(x)$, is derived from mass conservation:

$$V_\infty = U_\infty \frac{\mathrm{d}\delta^*}{\mathrm{d}x} + (\delta^* - h)\frac{\mathrm{d}U_\infty}{\mathrm{d}x}, \tag{3}$$

(where δ^* is the displacement thickness and h the domain height) and homogeneous Neumann conditions are applied to the fluctuating velocity components. This setup has already been successfully tested by De Prisco *et al* (2007) for the LES of an accelerating boundary layer in a configuration similar to the present one.

The numerical model used is a well-validated finite-difference code (Keating *et al* 2004b), based on a staggered grid. Second-order central differences are used for both convective and diffusive terms, and a semi-implicit time-advancement is used: the Crank–Nicolson scheme is used for the wall-normal diffusive term, while a low-storage third-order Runge–Kutta method is applied to the remaining terms. The Poisson equation is solved by a Fourier transform of the equation in the spanwise direction, followed by a direct solution of the resulting matrix, at each wavenumber, by cyclic reduction. The code is parallelized using the MPI protocol.

3. Rotating channel flow

The configuration for the plane channel flow subject to spanwise rotation is shown in figure 1(a). It is a canonical test case for turbulence models, since the interaction between wall turbulence and spanwise rotation plays an important role in turbomachinery, and has been studied experimentally (Johnston *et al* 1972) and numerically (Kristoffersen and Andersson 1993, Tafti and Vanka 1991, Piomelli and Liu 1995, Lamballais *et al* 1996). Due to the Coriolis force the flow becomes strongly asymmetric with respect to the plane $y = 0$. Turbulence is reduced on the cyclonic (stable) side (where the mean spanwise vorticity $\Omega_z = -\mathrm{d}U/\mathrm{d}y$ and the imposed rotation Ω have the same sign) and enhanced on the anticyclonic (unstable) one. At high rotation rates, partial or total relaminarization of the flow is observed on the cyclonic side. Turbulence models for the RANS equations have difficulties

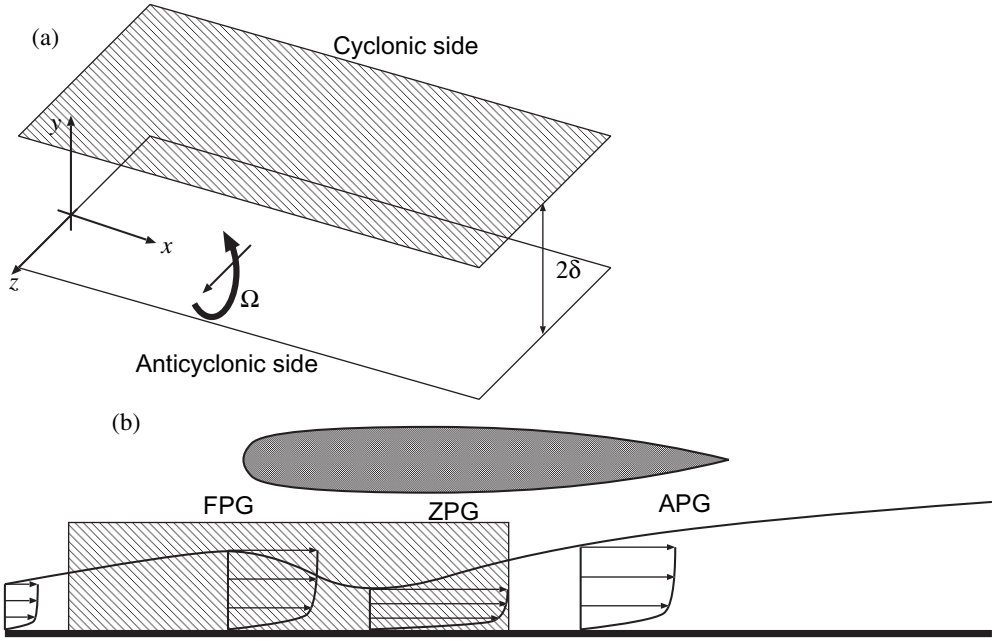

Figure 1. Sketch of the two numerical problems. (a) Rotating channel and (b) accelerating boundary layer. In part (b), the hatched region shows the computational domain. FPG refers to a region of favourable pressure-gradient, ZPG to zero pressure-gradient and APG to an adverse pressure-gradient.

predicting this phenomenon, while LES have been more successful when models were used in which the eddy viscosity vanishes in laminar flows (Piomelli and Liu 1995, Lamballais *et al* 1996). Calculations that modelled the SGS eddies with the Smagorinsky–Lilly model (Smagorinsky 1963, Lilly 1967) have been less successful (Tafti and Vanka 1991).

The relevant dimensionless parameters for this problem are the Reynolds number, $Re_\mathrm{b} = \delta U_\mathrm{b}/\nu$ (defined here using the bulk velocity U_b and the channel half-width δ), and the Rotation number $Ro_\mathrm{b} = \Omega\delta/U_\mathrm{b}$. Calculations were performed for $Re_\mathrm{b} = 5000$ and a range of rotation numbers. We will concentrate here on the case $Ro_\mathrm{b} = 0.21$. We performed numerical simulations with a computational domain size of $12\delta \times 2\delta \times 6\delta$; the DNS used $512 \times 192 \times 512$ cells, while the LES used $128 \times 96 \times 128$ (fine LES) or $96 \times 64 \times 96$ cells (coarse LES).

Firstly, simulations with no rotation were carried out. The results of both DNS and LES were in good agreement with the reference data, and with each other. Note that when no rotation is present, the Reynolds number based on the friction velocity is $Re_\tau \simeq 293$ for the DNS, and between 300 and 305 for the LES. This results in grid spacings in wall-parallel planes of $\Delta x^+ = 7$ and $\Delta z^+ = 3.5$ for the DNS, respectively, 28 and 14 for the fine LES, and 42 and 21 for the coarse one. Table 1 summarizes the error in the prediction of the friction velocity. The error in the prediction of the wall stress is due to the marginal grid resolution: the mesh cannot resolve adequately either the quasi-streamwise eddies in the near-wall region (whose size is only 3–4 grid cells) or the outer-layer structures (since Δx is only 1/8 of the channel half-width, and the integral scale in the outer layer is marginally resolved, for the coarse LES). A coarse DNS performed using the same grid as the LES gives significantly larger errors: the use of the SGS model is definitely beneficial. The spanwise rotation was

Table 1. Friction velocity in the non-rotating channel.

Simulation	Model	Grid	Re_τ	$\tau_w/\tau_{w,DNS}$
DNS	–	$512 \times 192 \times 512$	294	1.00
LES	DEV	$96 \times 64 \times 96$	297	1.03
LES	DEV	$128 \times 96 \times 128$	303	1.07
LES	LDEV	$96 \times 64 \times 96$	299	1.04
LES	LDEV	$128 \times 96 \times 128$	304	1.07
Coarse DNS	–	$96 \times 64 \times 96$	310	1.12
Coarse DNS	–	$128 \times 96 \times 128$	316	1.16

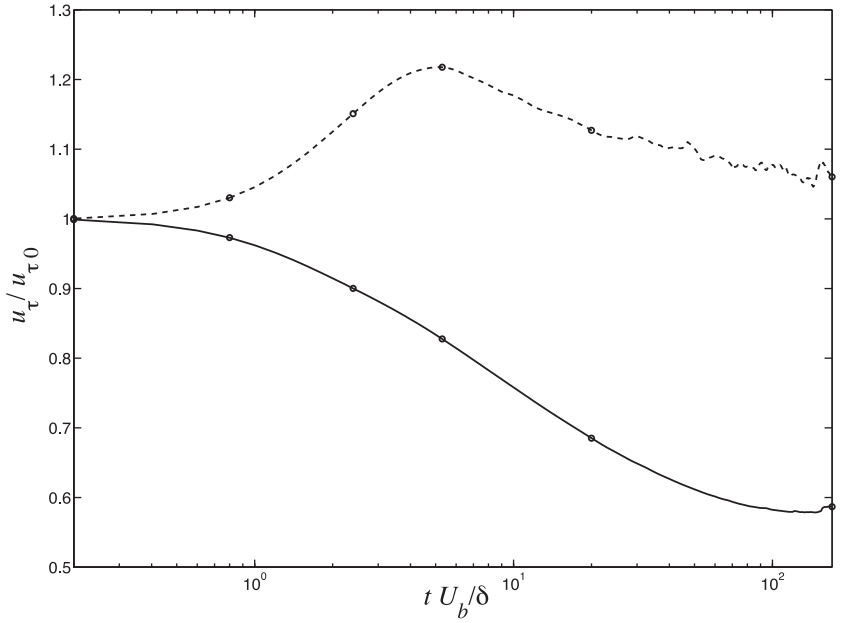

Figure 2. Time history of the friction velocity. DNS of the rotating channel. ——, Stable side; - - - -, unstable side.

then impulsively imposed, and the flow was allowed to develop and reach a steady state. The transient is as interesting as the final state, from the modelling point of view, since it highlights the response of the SGS eddies to the perturbation imposed through the rotation.

Figure 2 shows the time history of the friction velocity, $u_\tau = (\tau_w/\rho)^{1/2}$, on the two walls for the DNS (u_τ is normalized by its initial value). At steady state, the wall stress τ_w on the anticyclonic side is higher by approximately 20%, compared to the non-rotating case, while on the cyclonic side it is reduced by approximately 65%. The pressure gradient required to achieve the desired mass flux is 25% lower than in the non-rotating case. Note the overshoot of the friction velocity that precedes the steady state, and also the fact that the decrease of friction velocity on the stable (cyclonic) side is smoother and slower than the increase on the unstable side.

Figures 3(a) and (b) show the mean velocity profile and rms turbulence intensities obtained, at steady state, from the DNS and the two fine LES. The LES overestimate the wall stress by 30% for the coarse simulations and 25% for the fine ones; the error is larger on

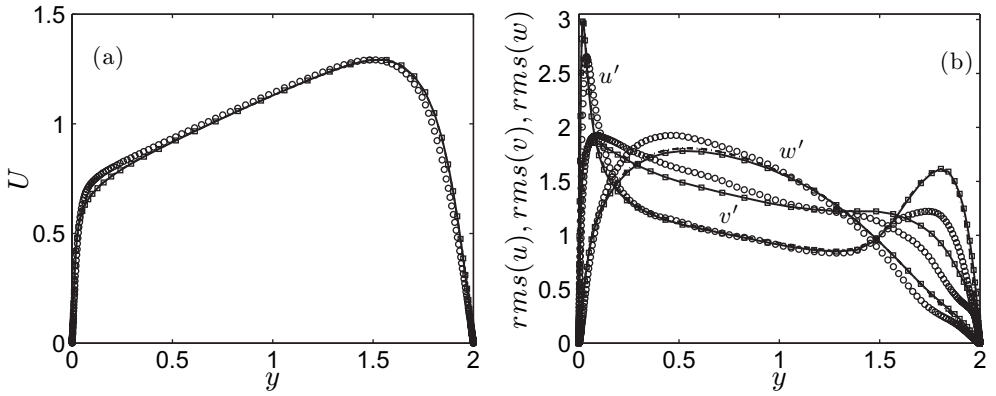

Figure 3. Turbulent statistics in the rotating channel. (a) Mean velocity profile. (b) Root-mean square fluctuation profiles. ○, DNS; —·—, fine LES, DEV model; □—□, fine LES, LDEV model.

the unstable side, where the local Reynolds number is up to 20% higher and more small scales are generated (and the grid becomes coarser, relative to the smallest scales present in the flow). The mean velocity profile, scaled with the bulk velocity, however, is in good agreement with the DNS data; differences in the profiles scaled in wall units can be attributed directly to the overprediction of u_τ.

We will now examine *a priori* the behaviour of the SGS stresses during the transient, focusing on the times indicated by a circle in figure 2, and compare it to actual LES results. The DNS velocity fields were filtered using a trapezoidal filter with filter width $\Delta_f = 4\Delta_g$ (where Δ_g is the grid size). The SGS stresses τ_{ij} and the SGS dissipation $\epsilon_{sgs} = -\tau_{ij}\bar{S}_{ij}$ ($\bar{S}_{ij}$ is the large-scale strain-rate tensor), which represents the net transfer of energy between resolved and subgrid scales, were then computed using the filtered data.

Figure 4(a) shows the resolved Reynolds shear stress and the SGS counterpart at four instants, ranging from the non-rotating regime (the initial condition) to the steady state. On the unstable side, the resolved stress increases and settles at a value larger than in the non-rotating case. The SGS stresses follow a similar trend. On the stable side, both resolved and SGS stresses decrease very rapidly; the peak Reynolds shear stress vanishes within a dimensionless time $tU_b/\delta = 2.4$ (equivalent to less than 0.2 large-eddy turn-over times $\delta/u_{\tau,o}$); the SGS stresses follow a similar trend. The modelled SGS stresses shown in figure 4(b) generally have the same behaviour predicted by the *a priori* study (the magnitudes are not expected to match, since the filter applied to the DNS data is not identical to that employed implicitly in the LES). The only significant difference between the *a priori* prediction and the results of actual calculation is observed at intermediate times ($tU_b/\delta \simeq 2.4$–6); here, the modelled stresses tend to be more confined to the near-wall region, perhaps due to the strong dependence of τ_{12} on the mean shear $\mathrm{d}U/\mathrm{d}y$. We again observe the delayed development of the SGS stresses on the unstable side when the LDEV model is used.

Figures 5(a) and (b) compare the response of resolved and SGS Reynolds shear stresses to the sudden imposition of the rotation. The plane-averaged model (DEV) shows a response that follows closely the *a priori* prediction of the DNS, while the Lagrangian-averaged version (LDEV) shows some delay of τ_{12} on the stable side, as well as a lower value of the same quantity at steady state on the unstable side. The first phenomenon is due to the fact that in the Lagrangian model the coefficient is obtained by averaging the model quantities over Lagrangian pathlines. When the rotation is imposed suddenly, the

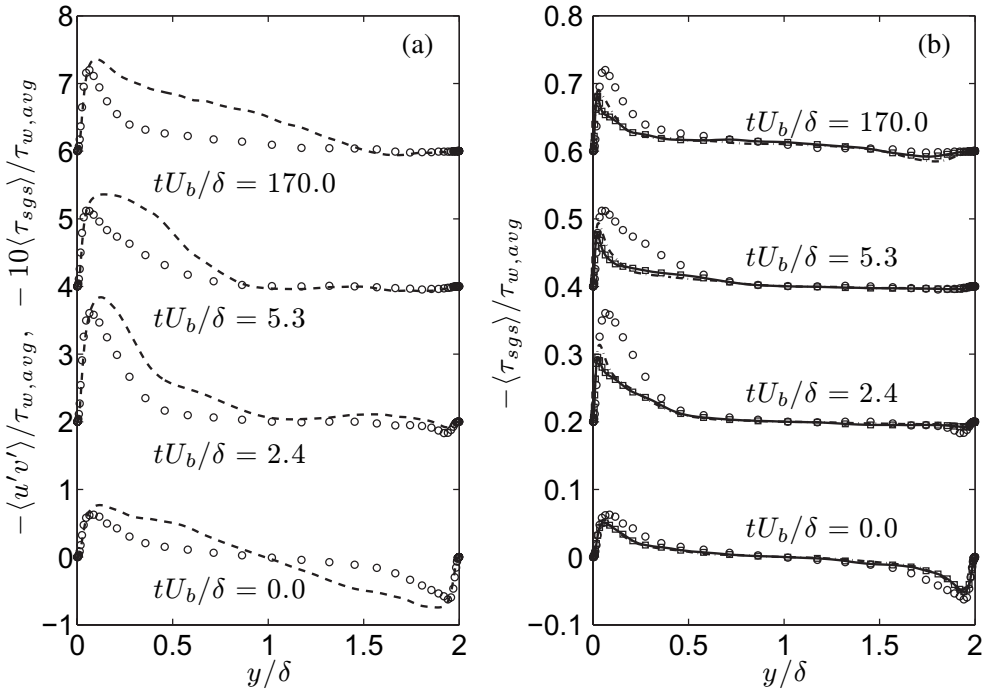

Figure 4. Reynolds and SGC shear stress, rotating channel. (a) *A priori* study: - - - -, resolved; ○, SGS. (b) *A posteriori* study: ○, exact SGS stress; —·—, DEV model; □—□, LDEV model. Note that the SGS stresses in part (a) have been multiplied by 10 for clarity.

plane-averaged model reacts instantaneously to the different state of the turbulence, while the LDEV model maintains some memory of the previous, non-rotating, state. The second effect is due to the fact that, at steady state, the LDEV model is not dissipative enough on the anticyclonic side, a well-known characteristic of this model when the resolution is marginal. A scale-dependent model such as that proposed by Porté-Agel *et al* (2000) may be beneficial in this situation.

Altogether, given how rapidly the transition from fully developed turbulence to a laminarescent state takes place, modelling errors are not very important in this flow. The most critical feature of the models tested here is their capability to make the eddy viscosity vanish when the resolved turbulence is damped out. The details of the decay of the stresses predicted by the SGS model may not be as important as the fact that the time scale of this decay is correct. This feature allows the flow on the stable side to be captured as long as there are no grid resolution issues.

4. Accelerating boundary layer

A boundary layer subjected to strong acceleration may revert to a laminar state. A decrease of the turbulence production is a significant cause of relaminarization in accelerating flows. This phenomenon is related to a reorientation of the quasi-streamwise vortices in the near-wall region and a decrease in the wall-normal momentum transport. This flow has been studied experimentally and numerically; a review of recent investigations can be found in De Prisco *et al* (2007). A typical setup for a numerical or experimental study of an accelerating boundary

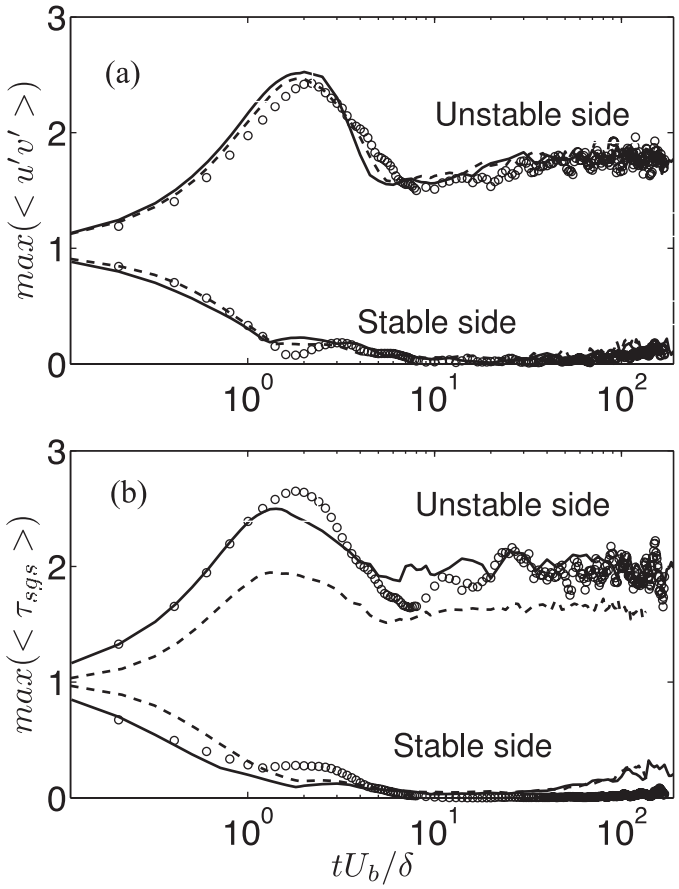

Figure 5. Temporal response of turbulence quantities. (a) Resolved stress; (b) maximum SGS stress. All quantities are normalized by their initial value. ○, DNS; ——, LES, DEV model; - - - -, LES, LDEV model.

layer is shown in figure 1(b). In experiments, the boundary layer on a flat surface is studied, and the pressure gradient is introduced by placing a contoured body above the flat surface, or by contouring the opposite wall of the wind tunnel. In our calculations, we directly impose a variable freestream velocity $U_\infty(x)$ on the top boundary of the computational domain (the hatched region in the figure), using the same freestream velocity distribution as De Prisco *et al* (2007) (shown in figure 6(a)). The acceleration parameter $K = (\nu/U_\infty^2)(\mathrm{d}U_\infty/\mathrm{d}x)$, shown in figure 6(b), exceeds significantly the threshold above which relaminarization is expected to occur ($K > 3 \times 10^{-6}$).

We considered two cases. In the first, the Reynolds number based on δ_o^* (the displacement thickness at a reference location, $x = 0$, located downstream of the rescaling plane) is 800 ($Re_\theta = 500$ based on momentum thickness θ). For the second case, we matched the conditions of case 2 in the experimental study of Warnack and Fernholz (1998), and used $Re_* = 1260$ and $Re_\theta = 865$.

At the lower Re we performed three calculations: a DNS using $4096 \times 257 \times 384$ grid points, and two LES with $1536 \times 192 \times 192$ points, one with the DEV model, the other with the LDEV one. The domain extended from $-60 < x/\delta_o^* < 540$; its height was $30\delta_o^*$ and its

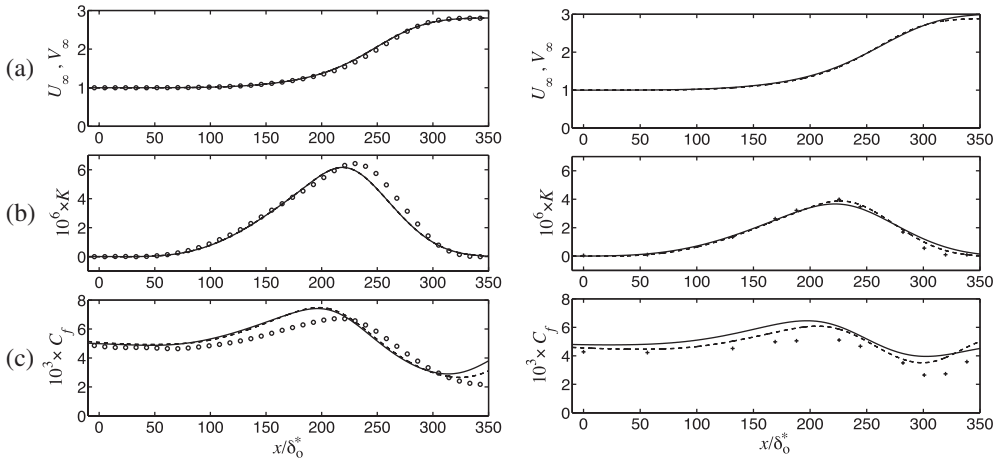

Figure 6. Streamwise development of (a) freestream velocity, (b) acceleration parameter and (c) skin-friction coefficient. FPG boundary layer. Left: $Re_* = 800$; ○, the DNS; — ·—, the LES, DEV model; ——, the LES, LDEV model. Right: $Re_* = 1260$; +, experiment (Warnack and Fernholz 1998); ——, LES, coarse mesh; - - - -, LES, fine mesh.

spanwise width was $20\delta_o^*$. The grid was equispaced in x and z, and stretched in the wall-normal direction y. The grid spacing in wall units is $5 < \Delta x^+ < 10$ and $2 < \Delta z^+ < 4.5$ for the DNS, whereas for the LES, $16 < \Delta x^+ < 35$ and $4.5 < \Delta z^+ < 10$. At the higher Re we performed two LES, both with the LDEV model, a coarse one with $1024 \times 124 \times 192$ points and a finer one with $1536 \times 144 \times 320$ points. The domain size was $488\delta_o^* \times 20\delta_o^* \times 28\delta_o^*$, with $-59 < x < 428$. The resulting grid spacing was $20 < \Delta x^+ < 40$ and $5 < \Delta z^+ < 10$ on the fine mesh and $30 < \Delta x^+ < 80$ and $10 < \Delta z^+ < 25$ on the coarse one. In both cases, downstream of $x = 350$, the grid becomes too coarse (in wall units), due to the increase in the friction velocity. All of the acceleration (and, therefore, the relaminarization) takes place within the useful region; the re-transition to a turbulent state begins at $x/\delta_o^* \simeq 300$ for all calculations.

To minimize any effect of the recycling conditions on the flow in the region of interest (where the pressure gradient is applied) a ZPG region is appended upstream of the beginning of the freestream acceleration. The recycling is performed within this inflow region (between two planes that are between 8 and 10 boundary-layer thicknesses apart); the flow is allowed to develop, in the ZPG region, for 5–10 boundary layer thicknesses before the acceleration is imposed. We also used the synthetic turbulence (Batten *et al* 2002) coupled with controlled forcing (Keating *et al* 2004a, 2006, De Prisco *et al* 2008) in the LES cases, and obtained results similar to the ones presented here.

The LES predict an early re-transition, beginning between $x = 300$ and 320, as shown by the increase in the skin-friction coefficient $C_f = \tau_w/(\rho U_\infty^2/2)$. This is consistent with the results of the study by Ovchinnikov *et al* (2004), who performed numerical simulations of bypass transition and observed that marginal mesh resolution resulted in early transition.

The *a priori* prediction of the SGS quantities is shown in figure 7. The SGS shear stress is initially significant through the lower third of the boundary layer. As the flow relaminarizes, the boundary layer becomes thinner, and τ_{12} decreases. At the beginning of re-transition the SGS stress increases again and remains confined to a thinner region near the wall (reflecting the lower boundary layer thickness in the re-transition region). The high values of τ_{12} observed

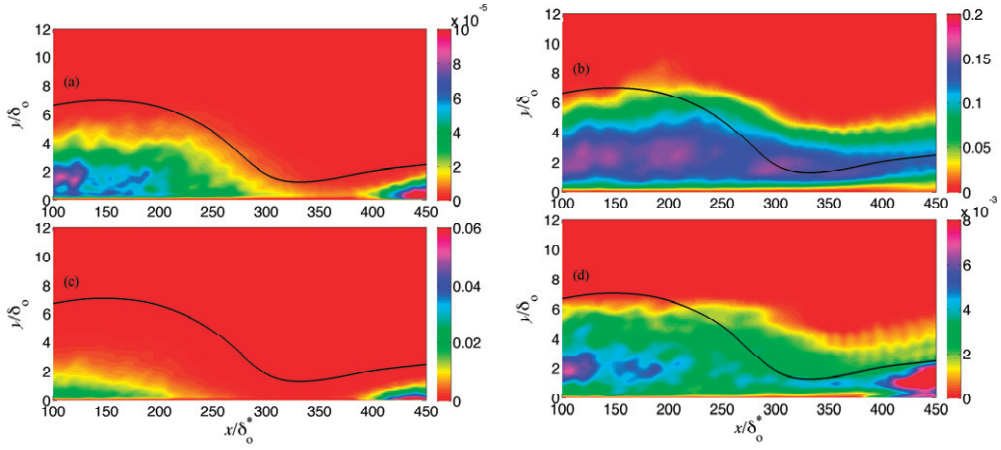

Figure 7. *A priori* prediction of the various measures of SGS activity. (a) SGS shear stress normalized by U_∞; (b) structure parameter a_1, defined in (4); (c) negative of the SGS dissipation $-\epsilon_{sgs}$, normalized by U_∞ and δ_o^*; (d) SGS structure parameter, $a_{1,sgs}$, defined in (5). The thick line shows the 99% boundary-layer thickness.

in the re-transition region are due to the fact that the Reynolds number here is higher (since U_∞ and u_τ are nearly three times larger than in the inflow region), and a wider range of scales is formed; since the filter size is the same as in the ZPG region, however, the expanded unresolved-scale range will increase the SGS contribution to momentum transport. The SGS dissipation follows similar trends; the effect of the shear, however, is to confine ϵ_{sgs} closer to the wall, compared to τ_{12}.

The structure parameter is defined as

$$a_1 = -\langle u'v' \rangle / q^2, \tag{4}$$

where $q^2 = \langle u_i' u_i' \rangle$; its SGS counterpart is

$$a_{1,sgs} = -\langle \tau_{12} \rangle / q^2. \tag{5}$$

These quantities are also shown in figure 7. In the ZPG region, a_1 has its expected value, equal to approximately 0.15. At relaminarization this value increases slightly and remains elevated at the beginning of transition. Note that here the region of significant a_1 extends well out of the boundary layer, and begins further away from the wall than in the initial equilibrium ZPG flow (two items worthy of further investigation). The behaviour of the SGS structure parameter $a_{1,sgs}$, although generally similar to that of a_1, also shows some differences. Its value, as expected, is significantly lower (the SGS stress with this filter is about 5% of the resolved one). It also decreases as the acceleration begins: by $x/\delta_o^* \simeq 200$ its maximum value is reduced by 50% (while the maximum value of a_1 has increased by 20%). This reflects the fact that the small scales decay more rapidly than the large ones (which determine the resolved stress and q^2). After re-transition begins, $a_{1,sgs}$ increases rapidly because of the increased SGS contribution to the momentum transport.

Profiles of mean velocity (normalized by the freestream velocity U_∞) as a function of y/θ are shown in figure 8. The LES agree fairly well with the DNS. Note the existence of a logarithmic layer in the initial ZPG region, followed by a region in which a well-mixed layer is established with a higher value of the von Kármán constant, as observed in other studies (see, for instance, De Prisco *et al* (2007)). The region of relaminarization is characterized by

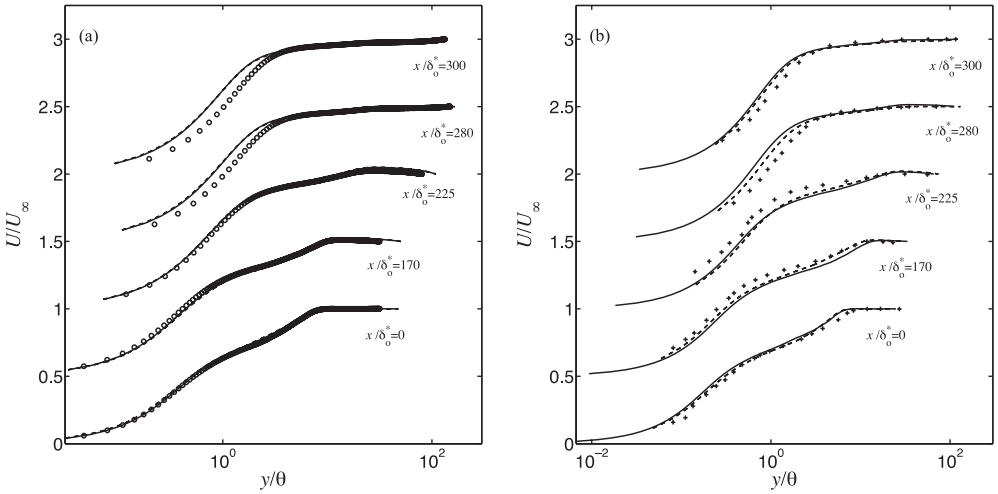

Figure 8. Mean velocity profiles. (a) $Re_* = 800$; ○, DNS; - - - -, LES, DEV model; ——, LES, LDEV model. (b) $Re_* = 1260$; +, Experiment (Warnack and Fernholz 1998); ——, LES, coarse mesh; - - - -, LES, fine mesh.

a low value of the friction velocity, and a laminar-like profile ($x/\delta_o^* \simeq 280$–350). The same profiles, when plotted in wall units, show some discrepancy between LES and DNS results, due to the overprediction of the wall stress by the LES, which results in a lower intercept of the logarithmic layer. This is a fairly common outcome of numerical simulations with marginal resolution and low dissipation, such as the present case: the numerical scheme, which uses a staggered mesh, is fully conservative, and the SGS models used are not very dissipative. Also note that, at the higher Re, the mean velocity obtained with coarse and fine grids collapses (although some difference was observed in the C_f, figure 6(c)), indicating reasonable grid convergence.

The prediction of the Reynolds stresses by the LES is also reasonably good. Figure 9 shows the streamwise turbulent intensities at several locations in the boundary layer. At $Re_* = 800$, the decrease of the rms intensity through the initial part of the acceleration region is predicted well. After $x/\delta_o^* = 250$, the peak rms is underpredicted by both LES models. At the higher Re, the discrepancies between LES and experiments also become significant around $x/\delta_o^* = 250$. Both the high-Re LES are coarser than those at low Re, in wall units, so that larger errors can be expected. The solution appears to be quite insensitive to the model at the resolution used.

Figure 10 shows the development of the negative of the SGS dissipation, $-\epsilon_{sgs}$, normalized by the local freestream velocity and momentum thickness. The DEV model is slightly more dissipative than the Lagrangian-averaged counterpart. The LDEV model, however, has a more realistic response to the acceleration: we observe a significant decrease of SGS activity, which mimics the decreased Reynolds stresses observed in this region as turbulence becomes inactive (see the discussion of this issue in Narasimha and Sreenivasan (1979) and also in De Prisco *et al* (2007)). The plane-averaged model, on the other hand, predicts significant dissipation in the region $200 < x/\delta_o^* < 300$, where very little production is observed, and turbulence is only advected. The DEV model predicts increased dissipation in the region where the flow re-transitions, small scales are generated, and the grid becomes excessively coarse (relative to the smallest scale present in the flow).

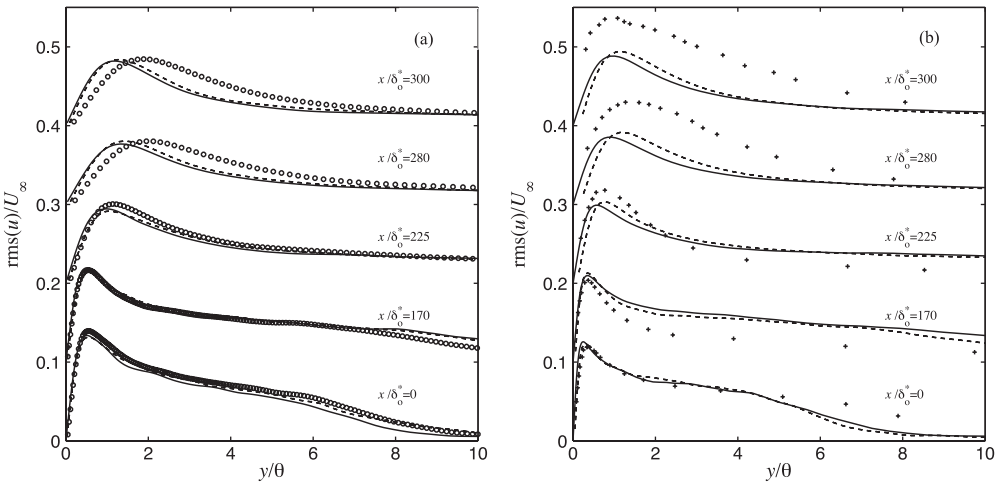

Figure 9. Profiles of the streamwise rms velocity. Left: $Re_* = 800$; ○, DNS; - - - -, LES, DEV model; ——, LES, LDEV model. Right: $Re_* = 1260$; +, Experiment (Warnack and Fernholz 1998); ——, LES, coarse mesh; - - - -, LES, fine mesh.

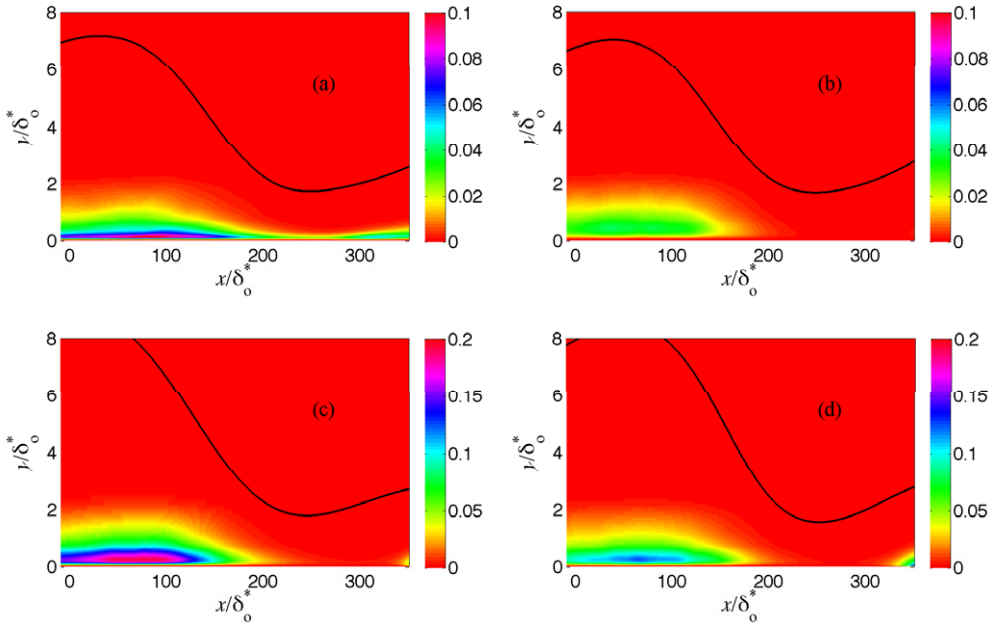

Figure 10. Contours of the negative of the SGS dissipation. (a) $Re_* = 800$, DEV model; (b) $Re_* = 800$, LDEV model; (c) $Re_* = 1260$, LDEV model, coarse grid; (d) $Re_* = 1260$, LDEV model, fine grid. The thick line represents the 99% boundary layer thickness.

In this flow, in which there is no homogeneity in the streamwise direction, one would expect the plane-averaged model (DEV) to give results that are much less accurate than the Lagrangian-averaged one (LDEV), in which the model coefficient depends more strongly on location. The DEV model, in this case, behaves like a constant-coefficient model in which the wall treatment is incorrect (such as the Smagorinsky–Lilly one (Smagorinsky 1963, Lilly 1967)). Since the SGSs only contribute about 5% to the turbulent momentum transport,

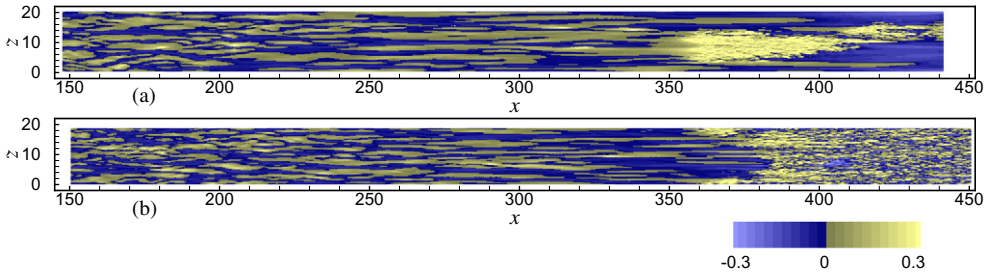

Figure 11. Contours of streamwise normalized velocity fluctuations u'/U_∞ in the $y/\delta_o^* = 0.1$ plane; $Re_* = 800$. (a) Fine LES; (b) DNS.

however, the modelling errors are not very significant, and the LES results turn out to be fairly insensitive to the SGS model used.

Generally, the LES predicts the relaminarization process accurately; not only are the statistical data predicted accurately, but the details of the process are also captured: the generation of elongated streaky structures in the relaminarization region, for instance, is predicted well. As can be expected, errors appear during re-transition, when the Reynolds number increases and the simulations lose resolution. In the DNS, for instance, transition develops through the appearance and growth of turbulent spots, as illustrated by the contours of the streamwise velocity fluctuations in a plane near the wall (figure 11), which highlight the appearance of a spot at $x \simeq 350$. In the LES, the gradual growth of turbulent spots is observed very rarely; transition between a perturbed laminar region and a fully turbulent one occurs more abruptly.

5. Conclusions

We have performed numerical simulations of two flows in which reversion from a turbulent to a laminar state occurs, in one case due to the Coriolis force and in the other case due to freestream acceleration. In both cases, we performed finely resolved DNS, which allowed us to study *a priori* the physical response of the unresolved scales, and also supplied data to evaluate the accuracy of SGS models, which were applied in actual LES.

The SGS models used (the plane-averaged DEV model and the LDEV model) do not predict the response of the SGS eddies precisely; however, the trends are correct (the eddy viscosity and SGS dissipation decrease in regions of reversion, for instance).

At the level of resolution used, the SGS contribution to the momentum transport was less than 10%, and the accuracy of the models tested was comparable. In the accelerating boundary layer case, the use of plane averaging is not justified, since the flow is highly inhomogeneous in the streamwise direction. However, because of the small contribution given by the SGS stresses to the turbulent momentum transport, the DEV model still gave results in good agreement with the DNS despite the known shortcomings of the model. Perhaps the most significant source of error, in the present LES, was the grid resolution, which resulted in high levels of turbulent activity near the wall; more dissipative models may be desirable to correct this error; the scale-dependent dynamic eddy-viscosity model (Porté-Agel *et al* 2000) may be a candidate.

While the relaminarization process was predicted well in detail, only the overall features of the re-transition were captured. This is not surprising, given the known sensitivity of this process to grid resolution. Even in this region, however, the LES predictions were reasonably accurate, given the coarseness of the resolution.

One limitation of the present study is the Reynolds number of the calculations. The desire to perform companion DNS limited the achievable Reynolds number. As a follow-up, we plan to perform simulations of the accelerating boundary layer and rotating channel at higher Reynolds numbers, for which experimental data are available, and evaluate the SGS models *a posteriori*.

Acknowledgments

We acknowledge the High Performance Computing Virtual Laboratory (HPCVL), Queen's University site, for computational support.

References

Batten P *et al* 2002 LNS—An approach towards embedded LES *AIAA Paper* 2002–0427

De Prisco G *et al* 2007 Large-eddy simulation of accelerating boundary layers *AIAA Paper* 2007–0725

De Prisco G *et al* 2008 Improved turbulence generation techniques for hybrid RANS/LES calculations *J. Turbul.* **9** 5 (20pp)

Domaradzki J A and Adams N A 2002 Direct modelling of subgrid scales of turbulence in large eddy simulations *J. Turbul.* **3** 024

Germano M *et al* 1991 A dynamic subgrid-scale eddy viscosity model *Phys. Fluids* A **3** 1760–5

Johnston J P *et al* 1972 Effect of spanwise rotation on the structure of two-dimensional fully developed turbulent channel flow *J. Fluid Mech.* **56** 533–57

Keating A *et al* 2004a A priori and a posteriori tests of inflow conditions for large-eddy simulation *Phys. Fluids* **16** 4696–712

Keating A *et al* 2004b Large-eddy simulation of heat transfer downstream of a backward-facing step *J. Turbul.* **5** 020

Keating A *et al* 2006 Interface conditions for hybrid RANS/LES calculations *Int. J. Heat Fluid Flow* **27** 777–88

Kristoffersen R and Andersson H I 1993 Direct simulations of low-Reynolds-number turbulent flow in a rotating channel *J. Fluid Mech.* **256** 163–97

Lamballais E *et al* 1996 Effects of spanwise rotation on the vorticity straining in transitional and turbulent channel flows *Int. J. Heat Fluid Flow* **17** 324–32

Lamballais E *et al* 1998 Spectral-dynamic model for large-eddy simulations of turbulent rotating channel flow *Theor. Comput. Fluid Dyn.* **12** 149–77

Lilly D K 1967 The representation of small scale turbulence in numerical simulation experiments *Proc. IBM Scientific Computing Symp. on Environmental Sciences* pp 195–210

Lilly D K 1992 A proposed modification of the Germano subgrid-scale closure method *Phys. Fluids* A **4** 633–5

Lund T S *et al* 1998 Generation of inflow data for spatially-developing boundary layer simulations *J. Comput. Phys.* **140** 233–58

Meneveau C *et al* 1996 A Lagrangian dynamic subgrid-scale model of turbulence *J. Fluid Mech.* **319** 353–85

Narasimha R and Sreenivasan K R 1979 Relaminarization of fluid flows *Advances in Applied Mechanics* vol 19 (New York: Academic) pp 221–309

Orlanski I 1976 A simple boundary condition for unbounded hyperbolic flows *J. Comput. Phys.* **21** 251–69

Ovchinnikov V *et al* 2004 Inflow conditions for numerical simulations of bypass transition *AIAA Paper* 2004–0491

Piomelli U and Liu J 1995 Large-eddy simulation of rotating channel flows using a localized dynamic model *Phys. Fluids* **7** 839–48

Porté-Agel F *et al* 2000 A scale-dependent dynamic model for large-eddy simulation: application to a neutral atmospheric boundary layer *J. Fluid Mech.* **415** 261–84

Smagorinsky J 1963 General circulation experiments with the primitive equations. I. The basic experiment *Mon. Weather Rev.* **91** 99–164

Tafti D K and Vanka S P 1991 A numerical study of the effects of spanwise rotation on turbulent channel flow *Phys. Fluids* A **3** 642–56

Voke P R and Yang Z 1995 Numerical study of bypass transition *Phys. Fluids* **7** 2256–64

Warnack D and Fernholz H H 1998 The effects of a favourable pressure gradient and of the Reynolds number on an incompressible axisymmetric turbulent boundary layer. Part 2. The boundary layer with relaminarization *J. Fluid Mech.* **359** 357–71